Insights from topo-bathymetric and oceanographic dataset for coastal flooding studies: The French Flooding Prevention Action Program of Saint-Malo

Léo Seyfried[1,3], Laurie Biscara[2], Héloïse Michaud[1], Fabien Leckler[2,4], Audrey Pasquet[1], and Marc Pezerat[2]

[1]Shom, 42 Avenue Gaspard Coriolis, BP 45017 - 31032 Toulouse CEDEX 5, France
[2]Shom, 13 rue du Chatellier, 29200 Brest, France
[3]Exail robotics SAS, ZI Toulon EST, 262 Rue des Frères Lumière, 83130 La Garde
[4]France Energies Marines, 25 Avenue Alexis de Rochon, 29280 Plouzané, France

Correspondence: Héloïse Michaud : heloise.michaud@shom.fr

Abstract. The Action Program for Flood Prevention of Saint-Malo, France, requires the assessment of coastal flooding risks and the development of a local flooding warning system. The first prerequisite is a knowledge of the topography and bathymetry of the bay of Saint-Malo ; the acquisition of new multibeam bathymetric data was performed in 2018 and 2019 to densify existing topo-bathymetric datasets and produce two high resolution (20 m and 5 m) topo-bathymetric digital terrain models. Second, the hydrodynamics associated with coastal flooding were investigated through a dense and extensive oceanographic field experiment conducted during winter 2018-2019, using a network of 22 moorings with 37 sensors : the network included 2 directional buoys, 2 pressure tide gauges, 18 wave pressure gauges, 4 single-point current meters, 7 current profilers and 4 acoustic wave-current profilers from mid-depth (25 m) up to the upper beach and the dike system. The oceanographic dataset thus provides an extended overview of hydrodynamics and wave processes in Saint-Malo bay, from coastal up to over-flooding and over-topping areas. It helps to identify the physical drivers of the coastal flooding, and provides a quantification of their respective contributions. In particular, the wave processes at the foot of the protection structures can be observed: in this macro-tidal environment, during high spring tides, short and infragravity waves propagate up to the protection structures, while the wave set-up remains negligible, and overtopping by sea packs can occur. The combination of high-resolution topo-bathymetric and oceanographic datasets allows the construction, calibration and validation of a wave and hydrodynamic coupled model that is used to investigate more deeply flooding processes, and might be integrated in a future local warning system by Saint-Malo intercommunality.

The topo-bathymetric and oceanographic datasets are available freely at doi : https://doi.org/10.17183/MNT_COTIER_GNB_PAPI_SM_20m_WGS84, https://doi.org/10.17183/MNT_COTIER_PORT_SM_PAPI_SM_5m_WGS84 and https://doi.org/10.17183/CAMPAGNE_OCEANO_STMALO (SHOM, 2020a, b, 2021).

1 Introduction

1.1 Context

In the context of global warming, with a rising sea level and increased frequency of extreme events (Fox-Kemper et al., 2021), the growth of population and economic activity in areas at risk increases the vulnerability to coastal flooding (Crossland et al., 2005). Public policies need therefore to rely on scientific studies on coastal flooding risks in order to make the most relevant decisions on urban planning or safety.

In France, since the major coastal flooding event caused by the storm Xynthia (Bertin et al., 2012) in 2010, the government has strengthened policies to prevent the risk of coastal flooding. Shom (a public administrative institution supervised by the Ministry of the Armed Forces, www.shom.fr) develops, in collaboration with the French meteorological service Météo-France, the numerical forecasting systems that support the operational warning system for storm surges, in the scope of the HOMONIM project (Jourdan et al., 2020). At more local scales, territories develop initiatives that contribute to the french program 'Flooding Prevention Action Programs' (PAPI) that promotes a comprehensive and balanced flood risk management thought at the scale of a coherent risk area, with regard to the hazard and the territory's specificity. To increase scientific knowledge and public awareness of the coastal flooding hazard, Saint-Malo intercommunality urban area (SMA) has established a preliminary PAPI, in which the Shom participates, as a national expert in support of public policies for the sea and the coasts. The Shom's contribution is based on various actions including:

- the realization of in-situ oceanographic and bathymetric sea campaigns during the winter of 2018-2019 in order to obtain up-to-date Topo-Bathymetric Digital Terrain Models (TBDTMs) as well as a characterization of physical properties of the coastal zone;

- the creation of a 42-year climatological hindcast to enable the definition of criteria for classifying high-risk storms and the calculation of joint return periods for static water height and waves, to characterize meteocean conditions favorable to coastal flooding and define warning thresholds;

- the generation of a very high-resolution coupled modeling system in Saint-Malo to model the storm surge and to consider in the medium term, an operational local flooding forecast system

This document describes and analyzes the first action. The data acquired are a prerequisite for the following 2 actions.

Getting access to detailed topo-bathymetric data is already a priority for communities anticipating impacts and preparing strategies in response to coastal risks. As elevation data are critical to depict regions prone to climate change impacts, this need will keep on increasing. Building high resolution and up-to-date TBDTMs, combining very dense and recent measurements from both ship-mounted multibeam echosounder and airborne LIDAR (Light Detection and Ranging), has become a prerequisite for modeling and forecasting of hydrodynamic processes at local scale (Eakins and Taylor, 2010). Shom developed multi-scales DTMs along the metropolitan and overseas French coasts based on user's requirements (Biscara et al., 2016) and on previous works (e.g., Eakins and Taylor, 2010; Eakins et al., 2011; Eakins and Grothe, 2014). This nested products line

was intended to be implemented in coastal flooding forecast systems in the scope of HOMONIM (Jourdan et al., 2020) and TANDEM (Hébert et al., 2014; Maspataud et al., 2015) projects. However, their diffusion on Shom's data portal facilitated their use for many other marine environment issues such as ecology, erosion, geology purposes (e.g., Furgerot et al., 2019; Tawil et al., 2019; Famin et al., 2020; Tew-Kai et al., 2020).

Characterization of physical properties of the coastal zone is needed for coastal flooding hazard assessments, and is done by acquiring oceanographic observations of the water level variation (Melet et al., 2020). The water level variation is due to a complex combination of processes occurring in the open ocean (linked to the climate changes or the general ocean circulation) and in the coastal zone that will be discussed here. In the coastal zone, the processes influencing water levels are mainly caused by tides, trapped waves, atmospheric pressure and wind effects, steric effects, wave setup, swash, infragravity waves, and, more locally, river runoffs, basin oscillations and meteotsunamis (Woodworth et al., 2019; Dodet et al., 2019). Thus, assessing the flooding risk at a local scale requires the monitoring of several meteocean variables (water levels, currents and sea states) and quantifying some processes (like storm surge, offshore wave, wave set-up, infragravity wave, swash). Such monitoring requires the establishment of extensive oceanographic campaigns to evaluate and quantify the various processes which cause the floodings. Shom is the referent for water level observations along the French coast through the tide gauge network REFMAR, and conducts numerous oceanographic campaigns for coastal to littoral areas monitoring and model validation (Filipot et al., 2013; Dodet et al., 2018), making use of its expertise and ressources.

In order to improve the knowledge of coastal flooding risks in Saint-Malo bay, an extensive bathymetric and oceanographic campaign was performed in winter 2018-2019. This paper describes and gives an analysis of the topo-bathymetric and oceanographic data collected as a prerequisite to any research and development study on flooding processes or forecasts. The topo-bathymetric and oceanographic datasets are detailed in parts 2 and 3, respectively. Part 4 outlines how these datasets will be valued for the studies of oceanographic processes and their assessment by numerical modelling. Part 5 provides the datasets availability. Finally, part 6 gives conclusions and limitations of these datasets.

1.2 Field site

Saint-Malo bay is located in the southern part of the Norman-Breton gulf (Figure 1.a). This bay is subject to a semidiurnal mega-tidal regime (maximum tidal range of about 13 m, Shom 2015) and the estuarine conditions are modified by a tidal power plant (Cochet and Lambert, 2017). Tidal currents are oriented E-SE during the flow and W-NW during the ebb, the velocities ranging from 1 m/s in the bay to 5 m/s in the estuarine part (Dagorne, 1966, 1968). In most situations, the waves come from W-NW to N-NW directions, with significant wave heights up to 6 m offshore during winter storms. Due to the presence of numerous obstacles (islets, shoals, groins), the waves propagation in the bay is complex. Moreover, geomorphology is marked by the presence of sand and rocky areas in the shallow bay, and a mixture of gravel and pebbles offshore (Bonnot-Courtois, 2002) making the dissipation of waves by bottom friction non-homogeneous in the bay.

The meteorological conditions are characterized by the passage of low pressure systems and cold fronts (Caspar et al., 2007). These weather conditions generate storm surges and are accompanied by significant swells. Combined with high spring tides, these events can lead to coastal flooding (Cariolet, 2011). Despite an existing dike system in front of Saint-Malo (Bonnot-
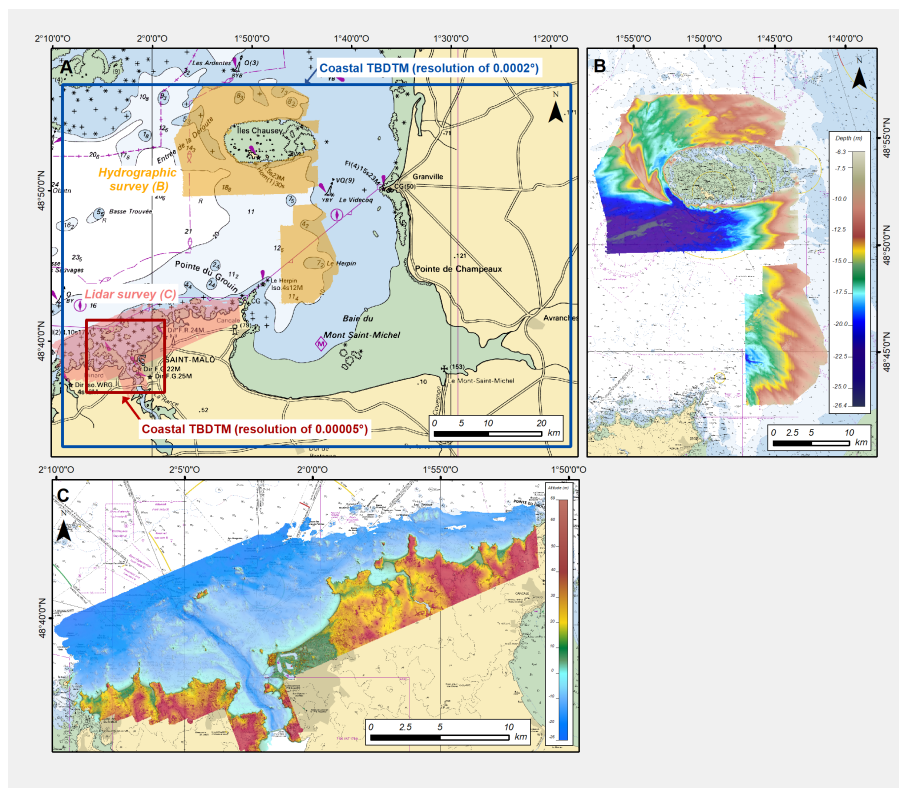
Figure 1. Nautical chart of Saint-Malo harbor and its surroundings (©Shom). (A) Locations of TBDTMs generated in the scope of Saint-Malo's PAPI project, (B) Hydrographic surveys carried out in the scope of PAPI Saint-Malo's project, (C) : Bathymetric coverage of Brittany v.20190831 Litto3D® maritime product of Saint-Malo harbor and its surroundings.

Courtois, 2002), 8 storms events resulting in flooding or/and damage on the nearshore zone have been recorded in the literature between 1979 and 2019, and more than 40 have been identified since 1703 (DHI, 2016).

2 Topo-bathymetric dataset

The purpose of the following sections is to present the different data used for the generation of the TBDTMs (Figure 1.a), the most common problems experienced with combining data and the approach adopted by Shom for their resolution (Maspataud et al., 2015; Biscara et al., 2016).

Table 1. Survey start and end dates for the 3 hydrographic surveys.

Hydrographic survey	Survey start date	Survey end date
La Pérouse (S201800400)	30/01/2018	22/03/2018
Laplace (S201805500)	19/09/2018	12/10/2018
Borda (S201901600)	26/03/2019	24/04/2019

2.1 Data sources

2.1.1 Specific Hydrographic Surveys

In the scope of the PAPI, the hydrographic vessels La Pérouse, Laplace and Borda were deployed between 2018 and 2019 in
95   the Normand-Breton Gulf in order to update areas characterized by poor hydrographic knowledge. The hydrographic surveys
covered approximately 230 km^2 in water depths ranging from -30 m to +6 m relative to the local chart datum (Figure 1.b).
Table 1 details the schedule of the 3 hydrographic surveys carried out as part of the PAPI.

The hydrographic vessels are equipped with a Kongsberg-Maritime EM710 multibeam echo sounder associated with the SIS
acquisition system. Depending on the vessel, sound velocity profiles were measured using Sippican XBT probes or a Valeport
100   SVP1000 Sound Velocity Profiler to correct bathymetric data for local variations in sound speed. Real time GPS positioning
was collected with the Applanix POS MV inertial unit. Positioning data were post processed in POSPac software using global
navigation satellite systems (GNSS) solutions. Horizontal positions were referenced to WGS84 or ITRF2014 geodetic systems
at the time of the survey.

The hydrographic surveys were processed and qualified according to the IHO S-44 standard in effect at the time of the
105   surveys were conducted (IHO, 2017a). Measured depths were corrected of various parameters (e.g. system calibration factors
and sensor offsets, attitude corrections, sound velocity or tide values for the reduction of soundings). Subset editing was carried
out by a qualified hydrographer (FIG/OHI/ICA cat. B, (IHO, 2017b)) using CARIS HIPS&SIPS 9.1 to remove systematic errors
and outliers. Processed and cleaned data were subjected to final validation by a senior qualified hydrographer (FIG/OHI/ICA
cat. A,(IHO, 2018)). The Total Vertical Uncertainty (TVU, (IHO, 2017a)) of these surveys at the 95% confidence level is equal
110   to 0.5 m. The Total Horizontal Uncertainty (THU, (IHO, 2017a)) at the 95% confidence level is between 0.55 m and 3.1 m.
Based on their characteristics, the 3 hydrographic surveys are compatible with orders 1a and 1b of the IHO S-44 standard.

2.1.2 Litto3D® program

LIDAR surveys exploited in this study were carried out within the framework of Litto3D® program. This national program
is based on a partnership between Shom and the French National Geographic Institute (IGN) (Louvart and Grateau, 2005).
115   It aims to provide very high resolution coastal altimetric models of metropolitan and overseas French coasts (Pastol, 2011).
Litto3D® surveys are regularly implemented on Shom's data portal (data.shom.fr) under Open Licence. Coastal mapping of the
Normand-Breton Gulf was performed by Shom's Litto3D® team between 2016 and 2018, covering approximatively 700 km2

and reaching up to 18 m water depth (Figure 1.c). Topo-bathymetric data were acquired from a Cessna Grand Caravan 208B type aircraft equipped with an airborne lidar topo-bathymetric HawkEye III double hatch (Leica Geosystems). The data were acquired in relation to the ellipsoid and referenced horizontally with respect to the RGF93 in standard UTM 30N projection. The trajectory of the aircraft was based on the GNSS system and processed by Inertial Explorer. The trajectory data were post-processed using the stations of the RBF (Réseau de Base Français). The points were generated from the processed waveform with Lidar Survey Studio (LSS) and the point cloud was processed using PFMABE version 6.4.0.43 tools. The validation of the cleaned data was finally done by qualified hydrographers. Final point cloud data were finally reported to the IGN69 altimetry reference frame and to the Lambert 93 projection by the Circe Batch (V4-3, Using RAF09 model) conversion tool.

2.1.3 Shom's bathymetric database

Complementary bathymetric data used to generate the TBDTMs were extracted from the Shom's bathymetric database (SBDB). 52 hydrographic surveys (490 millions of soundings) conducted between 1829 and 2019 with different sounding methods (lead-lines, single beam and multibeam echosounders) were available on the area of interest. Each survey extracted from the BDBS is associated with metadata, including the acquisition and processing methods, the IHO order survey and the quality of the data. Spatial coverage of each survey is represented as a vector polygon layer (called hereafter bounding polygon) that may adjoin, overlap or supersede older hydrographic surveys.

2.1.4 Other data

In addition to these bathymetric data, a bathymetric survey of the inner harbor delivered by the harbor authority of Saint-Malo was used in the present study. The bathymetric survey was carried out in June 2016 by the GEOXYZ society with a multibeam echosounder. Soundings were vertically referenced to the chart datum of Saint-Malo. This bathymetric source was evaluated prior to integration to other datasets.

The RGE ALTI® V2.0, produced by IGN, was exclusively used for the terrestrial domain. The data are available on the IGN's data portal (https://geoservices.ign.fr) in the RGF93 geodetic system, Lambert 93 projection. Vertical datum of the data corresponds to the NGF-IGN69 legal system (IGN, 2018). The RGE ALTI® v2.0 products used in the TBDTMs cover the departments of Côtes d'Armor, Ille et Vilaine and Manche at a resolution of 5 m. Data was clipped with a buffer extending to 3 km inland. Water-surface values were also eliminated using the raster layer of sources provided with the DTMs.

2.2 Production process

2.2.1 Convert data to a common horizontal and vertical datum

The key requirement for creating a seamless merged product is the homogeneity of the input datasets in terms of horizontal and vertical datum (Gesch and Wilson, 2001). The vertical transformation to the ellipsoid was performed with Circe 5.1 France (IGN) and Bathyelli V2.0 (Shom) for topographic and bathymetric data, respectively.

2.2.2   Conflict resolution

Selecting the most reliable source from multi-temporal and multi-sensor data is a fundamental challenge addressed in numerous
150 works (Macnab and Jakobsson, 2000; Wong et al., 2007; Maspataud et al., 2015). This issue is particularly true for hydrographic
offices, whose data legacy may be substantial: Shom's hydrographic knowledge counts presently more than 10,000 bathymetric
surveys conducted between 1816 and 2019 with many areas characterized by overlapping surveys. Survey depth measurements
were collected with different sounding methods and positioning systems whose accuracy has improved over time. Moreover,
the data may span decades, introducing temporal and geomorphologic change as a source of error (Eakins et al., 2011).

155   Due to the scarcity and the difficulty of collecting bathymetric data, bathymetric products are generated through a process
of data fusion with mixed levels of quality. To date, the selection of the most reliable surveys (i.e. conflict resolution) for the
production of nautical charts or TBDTMs was performed manually. This step is particularly time-consuming, especially in
regularly surveyed areas (Maspataud et al., 2015). In order to limit this fastidious work, Shom initiated in 2019 the Téthys
project (Figure 2). This in-house project aimed at constituting Shom's bathymetric reference surface for which source data
160 have been selected in order to generate the most accurate and up-to-date surface, satisfying the criteria related to the safety of
navigation (Le Deunf et al., 2023). The conflicts linked to overlapping surveys is resolved according to the qualitative elements
carried by the metadata (age, IHO survey order ...) which define if a survey supersede or complete older ones (Figure 2.b).
In case of a survey with a "supersede" status, the deconfliction process is executed by clipping the bounding polygon of the
reference survey to all other older overlapping surveys. No clipping is done for surveys with a "complete" status (Figure 2.b).
165 The implementation of many expert rules in the Tethys workflow and the comparison of the resulting bathymetric surface with
the nautical charts in use guarantee the consistency of the data. The resulting layer will be regularly updated on the basis of
newly integrated surveys (Figure 2.c). The Téthys project offers each operator data where their interactions are validated and
verified by a set of attribute rules and priority constraints related to each other (Le Deunf et al., 2023).

     The generation of TBDTMs in the Normand-Breton gulf benefited from the reliability of all metadata and bounding polygons
170 in the area of interest, which constitute the preliminary step prior to the construction of the Téthys. The deconfliction process
was executed on all datasets used for the generation of the TBDTMs using a semi-automated procedure based on GMT routines.
For the datasets not integrated in the SBDB for which no status exists, this one was directly defined by the operator on the basis
of inherent criteria of the data. The result of the deconfliction process corresponds to the most reliable soundings that can be
used as input into the surface modeling.

2.2.3   Interpolation

175

Because multiple sources of data contribute to the construction of the DTM, some datasets have data point spacing larger
than the required cell size. Splines functions are generally used for their efficiency to honour variable density data providing
a representative smooth and continuous surface. There may be more appropriate for large interpolation distances, which is
frequently required for bathymetric data (Amante (2012) and references therein). Based on these observations, Shom used
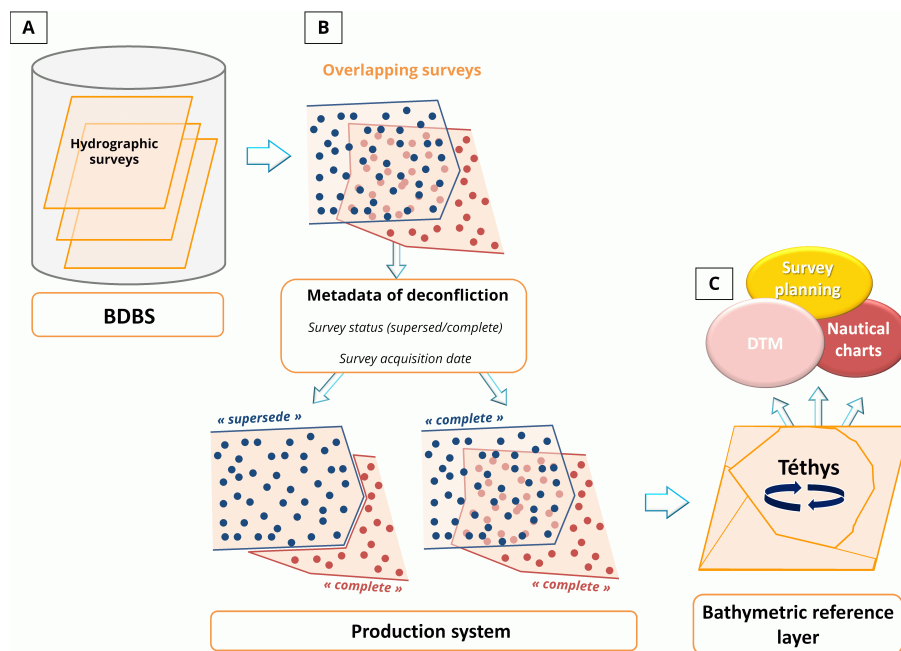
Figure 2. Workflow of Shom's bathymetric reference layer (« Téthys »). (A) Shom's hydrographic knowledge is composed of numerous overlapping surveys that are compiled in the BDBS. (B) In the case of overlapping surveys, a conflict resolution is applied based on the metadata of deconfliction. For bathymetric surveys which supersede older ones, the bounding polygon is used to clip the data. For bathymetric surveys which complete older ones, no action is performed. (C) Deconflicted data are compiled in one bathymetric reference layer for different applications. The reference layer will be updated each time a new survey is integrated in the BDBS.

180   the SAGA (System for Automated Geoscientific Analyses; Conrad et al. (2015)) software packages for the generation of the TBDTMs. Multilevel B-splines interpolation tool was used to perform surface modelling of the compiled data.

2.2.4 Altimetric conversion grids

Following NOAA's previous works (Eakins and Taylor, 2010; Eakins et al., 2011), different datum altimetric grids were developed by Shom to convert the TBDTMs from the ellipsoid to other tidal datums (Lowest Astronomical Tide and Mean Sea
185   Level).

2.2.5 Evaluation

The various evaluations carried out on the Tethys surface (reliability of attributes and bounding polygons, spatial coherence...) provide a coherent bathymetric surface. DTM coherency is equally evaluated based on visual inspection (slope, cross-section and 3D views) and through additional layers (density, sources diagram). If possible, a cross-validation of the DTM with datasets
190   that have not been incorporated into the generated product due to diffusion constraints is made. Despite the processing efforts

and the deconfliction process, erroneous representation of the sea-floor may remain. Preliminary versions of the TBDTMs highlighted two different types of artifacts:

– the overlapping of some bathymetric surveys with a "complete" status, leading to a noisy representation of the seafloor. In this case, the surface will not be suitable for modeling purposes despite the consistency of the surveys with each other in respect to the S-44 standard. Therefore, the survey with the strongest TVU is clipped to generate a smooth surface.

– Oscillation effects characterized by edge effects or topographic creep generated by spline interpolation into unsurveyed marine areas (Eakins and Grothe, 2014; Danielson et al., 2016). These unwanted surface artefacts can be reduced by using locally an appropriate tension factor.

As long as anomalies are detected, their cause must be determined and data reprocessed prior to a new interpolation. These different steps must be repeated iteratively until a satisfactory result is reached (Eakins and Taylor, 2010).

3 Oceanographic dataset

The oceanographic dataset includes water levels, currents and sea states observations from extensive in situ measurements conducted by the Shom during winter 2018-2019, using different types of sensors. In the following the field campaign and the data processing are described.

3.1 Oceanographic Surveys

From October 2018 to April 2019, an extensive oceanographic campaign was conducted in Saint-Malo bay. The campaign includes 22 moorings, each mooring containing one or two sensors, for a total of 37 sensors :

– Two directional waveriders (Datawell, DWR-MkIII, hereafter referred to as Datawell)

– Two tide pressure gauges (Seabird Electronics, SBE26+, hereafter referred to as SBE)

– Four acoustic wave and current profilers (Nortek, AWAC 600 kHz, hereafter referred to as AWAC)

– Four single-point current meters (Nortek, Aquadopp single-point current meter, hereafter referred to as Aquadopp)

– Seven current profilers (Nortek, Aquadopp profiler 1 MHz, hereafter referred to as AquaPro)

– Eighteen wave pressure gauges (Ocean Sensor System Inc., ten OSSI-010-003C and eight OSSI-010-022, hereafter referred to as OSSI and OSSI-NEW, respectively)

The moorings were located so as to accurately describe hydrodynamic conditions from offshore to the coastline (Figure 1). The Datawell were deployed offshore at 25 m-depth (Sauvages and Trouvée, Figure 1.a), providing information on the incident wave fields. Other moorings were essentially deployed along four cross-shore transects (T1, T2, T3 and T4, figure 1.b). Around the transects T1, T2 and T3, the beach profile is characterized by a gentle foreshore slope (2 %, Figure 1.c), increasing slightly
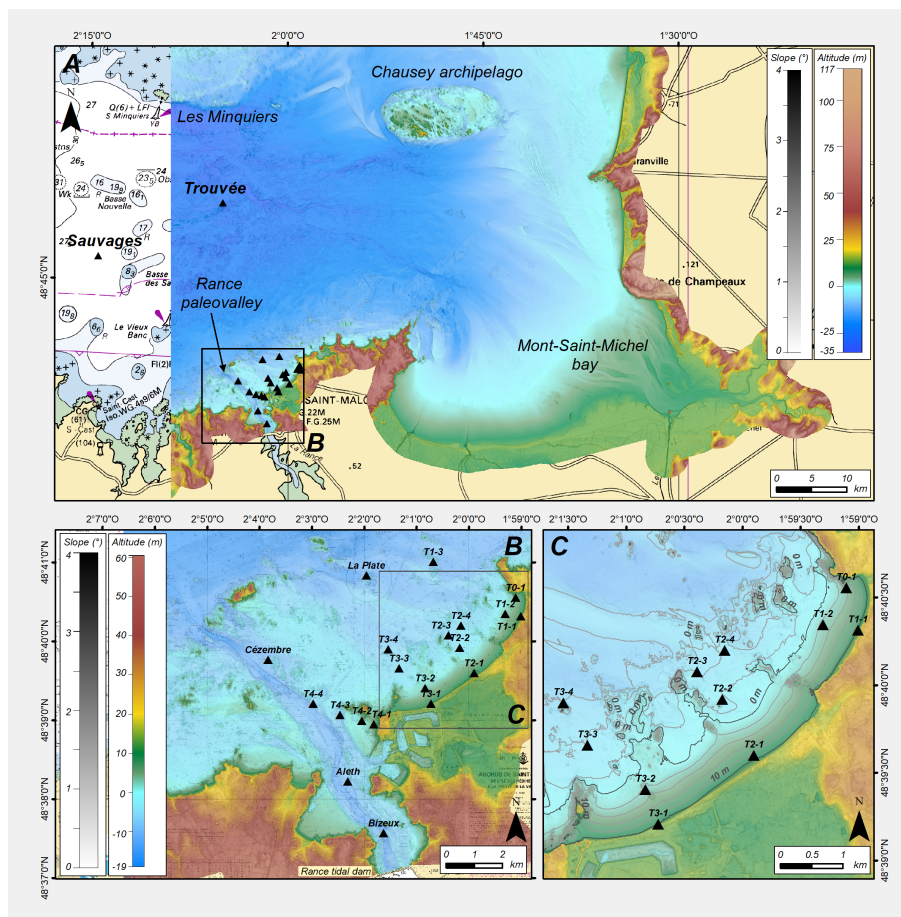
Figure 3. Nautical charts of Saint-Malo bay and its surroundings (©Shom). (A) coastal TBDTM covering a part of the Normand-Breton gulf at a resolution of 0.0002° (~20 m and moorings positions); (B) coastal TBDTM of the harbor of Saint-Malo and its surroundings at a resolution of 0.00005° (~5 m) moorings positions. (C) Zoom on the sensors transects.

(3 %) on the eastern part of the Minihic beach (T0 sensor). Transect T4 is located in the vicinity of the Grand Bé islet and is
220   characterized by high slope variations due to the presence of the Rance estuary (Figure 1.b). Two moorings, with OSSI and AquaPro, were deployed in the Rance estuary (Bizeux and Aleth Figure 1.b). Table 2 summarizes the location of each mooring and sensor. For consistency with TBDTMs, the vertical datum used is the Lowest Astronomical Tide (LAT).

Table 2. Moorings and sensors location.

Moorings	Sensors	Latitude (WGS84)	Longitude (WGS84)	Sensors depth (LAT)	Heightfrombed
T0-1	OSSI	48.675893°	-1.985119°	-4.60 m	0.19 m
T1-1	OSSI	48.671880°	-1.983443	-10.58 m	0.15 m
T1-2	OSSI	48.672397°	-1.988447°	-3.98 m	0.35 m
	AquaDopp			-4.34 m	0.71 m
T1-3	OSSI	48.683417°	-2.011383°	6,00 m	0.32 m
	AWAC			5.70 m	0.62 m
T2-1	OSSI	48.659966°	-1.998369°	-9.17 m	0.11 m
T2-2	OSSI	4.665283°	-2.002883°	1.88 m	0.35 m
	AquaDopp			1.52 m	0.71 m
T2-3	OSSI	48.667900°	-2.006517°	4.09 m	0.35 m
	AquaPro			3.73 m	0.71 m
T2-4	OSSI	48.669933°	-2.002533°	4.72 m	0.35 m
	AquaPro			4.36 m	0.71 m
T3-1	OSSI	48.653437°	-2.012057°	-11.36 m	-
T3-2	OSSI	48.656722°	-2.013924°	-3.67 m	0.35 m
	AquaDopp			-4.03 m	0.71 m
T3-3	OSSI	48.660933°	-2.022233°	4.16 m	0.35 m
	AquaPro			3.80 m	0.71 m
T3-4	OSSI	48.664967°	-2.025683°	4.96 m	0.35 m
	AquaPro			4.60 m	0.71 m
T4-1	OSSI	48.649110°	-2.030283°	-5.93 m	0.20 m
T4-2	OSSI	48.649900°	-2.034132°	-4.60 m	0.35 m
	AquaDopp			-4.96 m	0.71 m
T4-3	OSSI	48.651117°	-2.041050°	5.26 m	0.35 m
	AquaPro			4.90 m	0.71 m
T4-4	OSSI	48.653483°	-2.049600°	5.77 m	0.35 m
	AWAC			5.50 m	0.62 m
Aleth	OSSI	48.637033°	-2.038617°	4.46 m	0.35 m
	AquaPro			4.10 m	0.71 m
Bizeux	OSSI	48.626167°	-2.027150°	9.36 m	0.35 m
	AquaPro			9.00 m	0.71 m
Cezembre	SBE	48.662700°	-2.063933°	6.00 m	-
	AWAC			5.90 m	0.62 m
La Plate	SBE	48.680533°	-2.032583°	5.17 m	-
	AWAC			6.20 m	0.62 m
Trouvée	DATAWELL	48.813183°	-2.083483°	25 m	-
Sauvages	DATAWELL	48.768550°	-2.242817°	25 m	-

Sensors deployed during the campaign have been programmed to accurately record the oceanographic data, taking into account battery and data storage limitations. Sensors settings in terms of measurement data, sampling rate, average interval

225 and measurement interval are summarized for each sensor in Table 3.

Table 3. Sensor acquisition protocol.

Moorings	Sensors	Datas	Sampling rate	Average interval	Measurement interval	Remarks
T0-1	OSSI	Bottom Pressure	10 Hz	Continuous		-
T1-1	OSSI	Bottom Pressure	10 Hz	Continuous		-
T1-2	OSSI	Bottom Pressure	10 Hz	Continuous		-
	AquaDopp	Current	-	120 s	600 s	-
		Bottom Pressure				
T1-3	OSSI	Bottom Pressure	10 Hz	Continuous		-
		Current	-	120 s	600 s	
	AWAC	AST	2 Hz	1024 s	7200 s	-
		Bottom Pressure	2 Hz	1024 s	7200 s	
T2-1	OSSI	Bottom Pressure	8 Hz	Continuous		Battery Problem
T2-2	OSSI	Bottom Pressure	8 Hz	Continuous		Battery Problem
	AquaDopp	Current	-	120 s	600 s	-
		Bottom Pressure				
T2-3	OSSI	Bottom Pressure	8 Hz	1800 s	3600 s	Battery Problem
	AquaPro	Current	-	120 s	1200 s	-
		Bottom Pressure				
T2-4	OSSI	Bottom Pressure	8 Hz	1800 s	3600 s	Battery Problem
	AquaPro	Current	-	120 s	1200 s	-
		Bottom Pressure				
T3-1	OSSI	Bottom Pressure	8 Hz	Continuous		Battery Problem Siltation
T3-2	OSSI	Bottom Pressure	8 Hz	Continuous		Battery Problem
	AquaDopp	Current	-	120 s	600 s	-
		Bottom Pressure				
T3-3	OSSI	Bottom Pressure	8 Hz	1800 s	3600 s	Battery Problem
	AquaPro	Current	-	120 s	1200 s	-
		Bottom Pressure				
T3-4	OSSI	Bottom Pressure	8 Hz	1800 s	3600 s	Battery Problem
	AquaPro	Bottom Pressure	-	120 s	1200 s	-
T4-1	OSSI	Bottom Pressure	10 Hz	Continuous		-
T4-2	OSSI	Bottom Pressure	10 Hz	Continuous		-
	AquaDopp	Current	-	120 s	600 s	-
		Bottom Pressure				
T4-3	OSSI	Bottom Pressure	10 Hz	1800 s	3600 s	Mooring Lost
	AquaPro	Current	-	120 s	1200 s	
		Bottom Pressure				
T4-4	OSSI	Bottom Pressure	10 Hz	1800 s	3600 s	-
		Current	-	120 s	600 s	
	AWAC	AST	2 Hz	1024 s	7200 s	-
		Bottom Pressure	2 Hz	1024 s	7200 s	
Aleth	OSSI	Bottom Pressure	10 Hz	1800 s	3600 s	-
	AquaPro	Current	-	120 s	1200 s	-
		Bottom Pressure				
Bizeux	OSSI	Bottom Pressure	10 Hz	1800 s	3600 s	-
	AquaPro	Current	-	120 s	1200 s	-
		Bottom Pressure				
Cézembre	SBE	Bottom Pressure	4 Hz	120 s	1200 s	-
		Current	-	120 s	600 s	
	AWAC	AST	1 Hz	1024 s	3600 s	-
		Bottom Pressure	1 Hz	1024 s	3600 s	
La Plate	SBE	Bottom Pressure	4 Hz	120 s	1200 s	-
		Current	-	120 s	600 s	
	AWAC	AST	2 Hz	1024 s	7200 s	Sensor disconnected
		Bottom Pressure	2 Hz	1024 s	7200 s	
Trouvée	DATAWELL	Displacement	1.28 Hz	Continuous		-
Sauvages	DATAWELL	Displacement	1.28 Hz	Continuous		-

3.1.1 Sensor acquisition

Figure 4 presents a summary report of sensor acquisition. All moorings, except buoys, started on november, the 12th 2018. The last acquisitions were around March 30 or April 20 for foreshore or offshore moorings, respectively. The acquisitions of Datawell buoys began on November 15, 2018, for Trouvée mooring and on December 2, 2018, for the Sauvages mooring,

230   until April 29, 2019, for both buoys. Figure 4 shows interruptions in data acquisition for OSSI-NEW in transects T2 and T3. These interruptions were caused by less efficient batteries than anticipated on the OSSI-NEW's (as mentioned in table 3). For moorings on the foreshore, a brief interruption in the data acquisition appeared from January 22 and January 24. This interruption was planned for a battery change. The "La Plate" AWAC sensor did not acquire any data during the campaign (the sensor power cable was disconnected). The mooring T3-4 with all the sensors remains unfortunately unrecovered, problably

235   due to a malicious act. Despite these incidents, the density and complementarity of the instruments used during the campaign give an homogeneous description of the hydrodynamics in Saint-Malo bay. The data collection covers a winter period of more than 4 months.
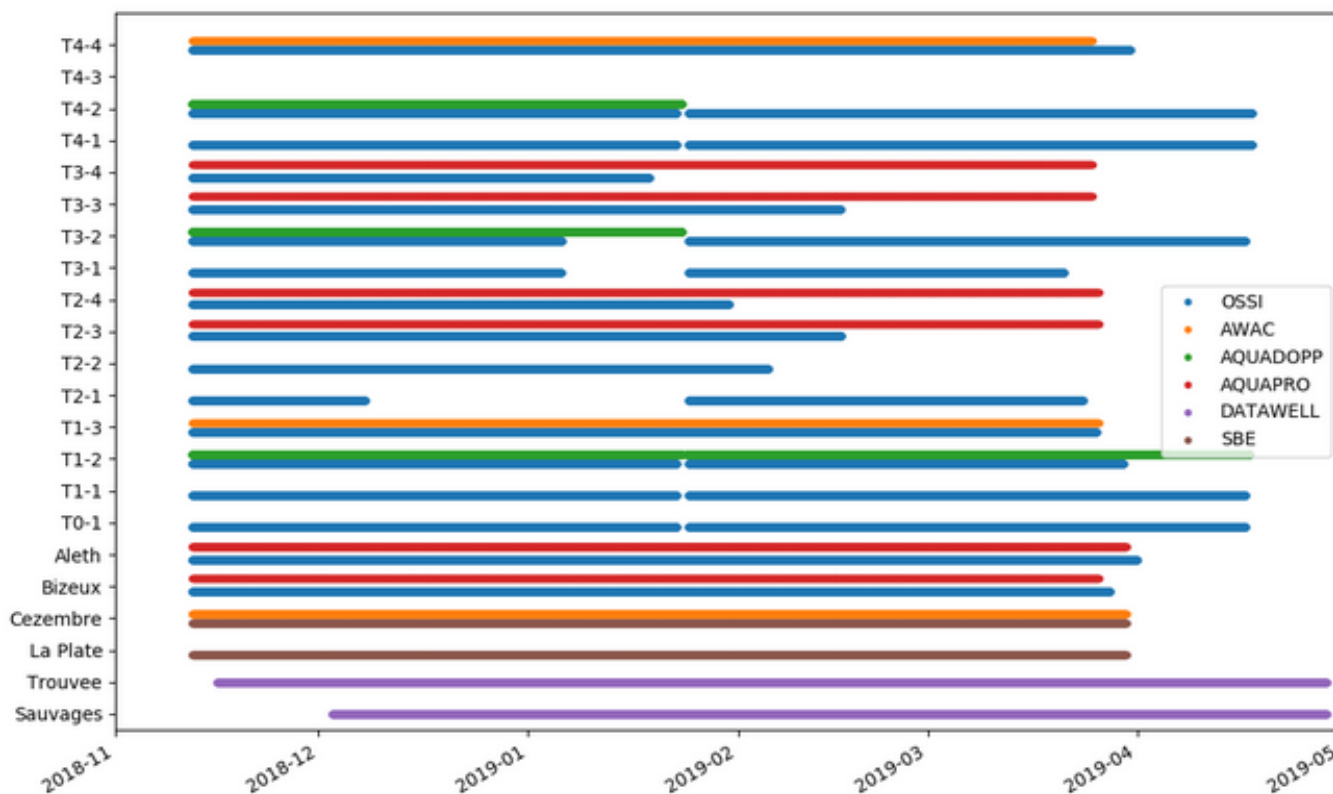
Figure 4. Moorings acquisition report.

3.2 Data processing

The workflow for generating the oceanographic dataset consists of three steps:

240
- Pre-process binary data using the manufacturers' software.

- Process the data using the Python toolbox SCOT developed for this study.

- Write data, metadata to netcdf format.

3.2.1 Water levels

The water levels are mainly monitored by pressure sensors including tide pressure gauge (SBE) and wave pressure gauge
245 (OSSI) using different sampling frequencies and acquisition plan (Table 3). Current meters (Aquadopp, Aquapro or Awac) are
also equipped with pressure sensors.

The tide pressure gauges also record the 2 min-averaged bottom pressure every 20 minutes. The raw data was converted in
water level h assuming hydrostatic equilibrium (Eq. 1):

$$250 \quad h = \frac{P_m - P_{atm}}{\rho g} + \delta_m \tag{1}$$

with P_m, the bottom pressure measurement in Pa, P_{atm}, the atmospheric pressure extracted from ERA5 atmospheric reanalysis in Pa, $\rho = 1026 \, \mathrm{kg}/m^3$, the averaged water density measured in Saint-Malo bay, δ_m the sensor's distance from bed in m
and $g = 9.81 \, \mathrm{m}/s^2$ the gravitational acceleration. Note that the data from ERA5 reanalysis were preferred to measurements at
Dinard airport meteorological station due to acquisition problems.

255

The wave pressure gauges and current meter with pressure sensors record bottom pressure at higher frequency (see Table
3). In case of continuous measurements, the data recorded in ascii format were aggregated in consecutive bursts of prescribed
length (20 min here). The raw pressure data of each sensor is calibrated using the pressure slope and offset of the sensor. For
foreshore sensors, the calibration is performed by comparing the burst-averaged pressure measured whenever the sensor is out
260 of water to the atmospheric pressure (e.g. see Appendix C). For offshore sensors, the pressure sensor was calibrated before
or at the end of the recording when the instrument was taken out of the water. Then, the corrected pressure was converted
into water level assuming hydrostatic equilibrium (Eq. 1). Finally, to reconstruct water level for the long waves such as tide,
the water level was smoothed, with moving average of 10 min, to filter out deformations of water surface related to short waves.

265 In order to compare water levels recorded from different instruments, the measurements were relocated in height with respect
to the tide gauge of Saint-Malo harbour (e.g. see Appendix C). The correction factors (slope and offset) from Saint-Malo tide
gauge is provided in the dataset for each sensor. The accuracy of water levels is in the order of ± 5 cm. For consistency with
TBDTMs, the vertical datum used is the Lowest Astronomical Tide (LAT).

Finally, acoustic surface tracking (AST) with vertical beam performed by AWAC current meters allow the sampling of the
270   surface elevation.

3.2.2 Currents

The currents are monitored by acoustic Doppler current using single-point current meters (Aquadopp) and current profilers
(AquaPro and AWAC). These sensors record the speeds in the axis of their three beams. The raw binary data file was directly
processed by the Python toolbox SCOT developed for this study. First, the velocity data are reprojected in a terrestrial landmark,
275   on the north-east-vertical axes. Prior to their deployment, the magnetic compasses of these current meters were previously cal-
ibrated on a dedicated Shom platform. The calibration procedure and the uncertainty of current data are described in Le Menn
and Morvan (2020). Finally the current data and metadata of each sensor are written in netcdf format.

3.2.3 Sea States

The sea states are monitored by three different types of sensor: directional wave buoy, wave pressure gauge, and acoustic wave
280   and current profiler.

The directional wave buoys recorded wave displacements in the three directions of the ENU frame using measurements from
accelerometers, inclinometers and compass. First, a quality control is performed on each 30 min bursts, such that a burst is
discarded if at least one of the three displacements is outside the range $\pm 4\sigma$ where σ is the standard deviation of the timeseries.
285   Then, the cross-spectra of the displacements were computed by means of a fast Fourier transform on 10 hanning-windowed
segments with a 50% overlap, which allows a good compromise between statistical stability (20 degrees of freedom) and
frequency resolution (5.5 mHz). The power spectral density of vertical displacements are used for estimating the main bulk
parameters (see Appendix B), while the five other independent co- and quad-spectra are used to compute the main directional
parameters and estimate the directional distribution using the Iterative Maximum Likelihood Method with an angular resolu-
290   tion of 5° (e.g., see Oltman-Shay and Guza, 1984) so as to compute an estimate of the directional spectra.

For the wave pressure gauges, the free surface elevation signal associated with waves was first reconstructed from bottom
pressure measurements so as to account for the non-hydrostatic effects. A recent review of Mouragues et al. (2019) provides
different methods depending on the assumptions made on the wave field's dispersive properties. In addition to the hydrostatic
295   reconstruction, the linear method and non-linear weakly dispersive method (see Appendix A) were thus applied on each burst
after detrending so as to suppress tidal motion. The wave spectra were computed as described above (resulting in 20 degrees
of freedom and a frequency resolution of 5.5 mHz) to finally compute spectral estimates of the bulk parameters in addition to
the wave-by-wave analysis (see AppendixB).

300   The AWAC records surface elevation from Acoustic Surface Tracking (AST) and the two components of the horizontal
current in the ENU frame within a sub-surface wave cell at high frequency. First, a quality control is performed on each burst

based on the QC-flag associated with AST measurements, such that a burst is discarded when the first quartile of the QC-flag distribution is below 100, which corresponds to the ceil below which the measurement is considered dubious (Nortek support team personal communication). Then, the cross-spectra of the measurements triplet were computed as described above
305   (resulting in 20 degrees of freedom and a frequency resolution of 7.8 mHz) and the same processing as for the directional wave buoy measurements is performed (e.g. see Krogstad et al., 1988, for the estimate of the directional distribution from ADCP measurements using the IMLM method).

4   Applications of these dataset

4.1   Overview of oceanographic processes
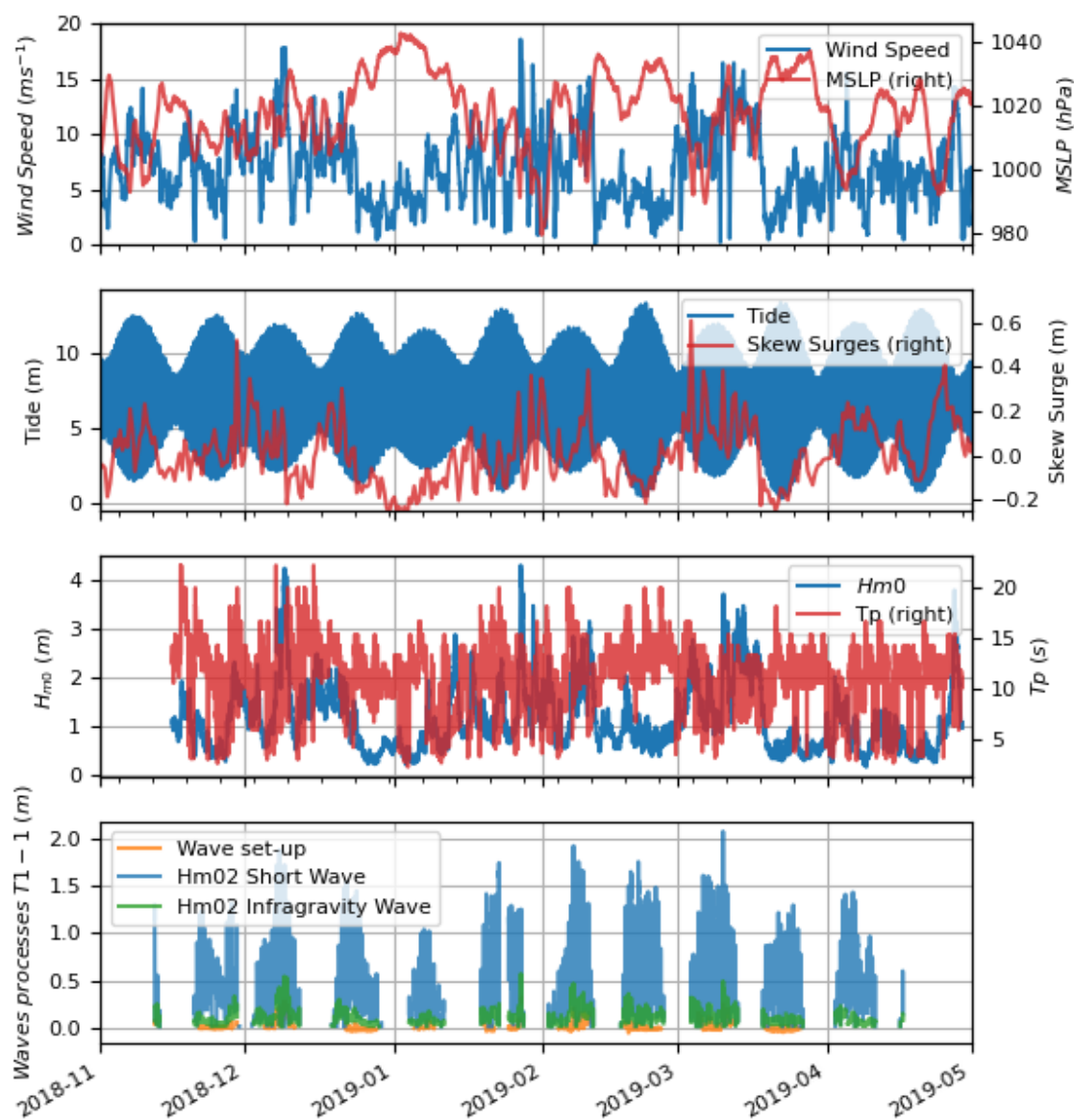
Figure 5. (A) wind speed and Mean Sea Level Pressure (MSLP) from ERA5 reanalysis in Saint-Malo. (B) Tide prediction and skew surge at Saint-Malo harbour tide gauge. (C) Significant wave height H_{m0} and peak period at Trouvée buoy. (D) Short and infragravity significant waves height, and wave set-up at T1-1 .
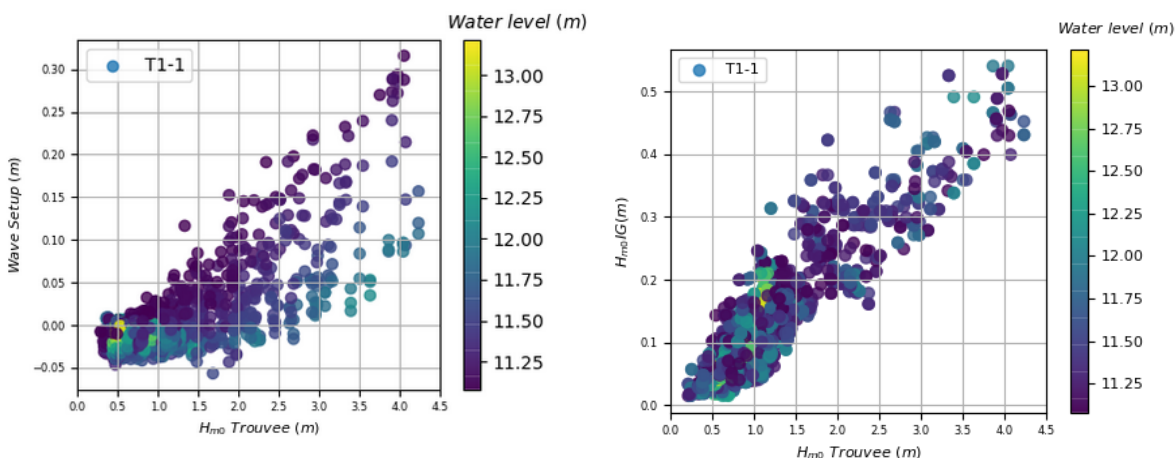
Figure 6. Wave set-up (left) and infragravity significant wave height (right) at T1-1 mooring according to offshore significant wave height and water level (color).

Table 4. Inventory of metocean conditions (Wave conditions at Trouvée) and waves processes at T1-1 during storm events and major spring tide events of field experiment.

	MSLP (hPa)	Wind speed (m/s)	Hm0 offshore (m)	Tp offshore (s)	Height Tide (m)	Skew Surge (cm)	Set-up (cm)	Short Waves (cm)	Infragravity Waves(cm)
29/11/18	1003	14	2.29	18	10.59	53	4	110	25
09/12/18	1011	18	4.24	11	11.80	22	27	173	54
27/01/19	991	18	4.28	11	10.91	29	32	128	52
10/02/19	996	15	3.08	8	10.98	39	15	130	24
21/02/19	1032	3	1.0	10	13.17	-10	0	136	12
03/03/19	994	15	2.75	14	10.01	61	-	-	-
10/03/19	1011	16	3.73	11	11.70	33	24	207	50
22/03/19	1030	4	0.7	14	13.33	-15	0	82	6

310 The figure 5A-C shows an overview of the temporal evolution of the metocean conditions during the studied period. First, several low-pressure systems affected Saint-Malo. These storm events produced skew surges (that is the difference between the maximum observed sea level and the maximum predicted tide regardless of their timing during the tidal cycle) from 22 cm to 61 cm and offshore significant wave heights from 2.29 m to 4.28 m. These storms occur principally during neap tides. No coastal flooding was observed during this experiment. The storm events associated with two major spring tides are reported in

315 Table 4 with the corresponding metocean conditions.

The wave transformation induces further processes affecting water level elevation such as wave set-up and infragravity waves (e.g. see Dodet et al., 2018). The figure 5D shows the wave set-up estimated from the difference of water level between sensor T1-1 and T1-2 and infragravity significant wave height (between 0.004 and 0.04 Hz) at T1-1. The maximum wave set-
320 up was measured during the 09/12/18, 27/01/2019 and 10/06/19 storms with wave set-up measurement of around 27 cm, 32 cm and 24 cm, respectively. The maximum infragravity significant wave heights also occur during these storms with heights greater than 50 cm. Table 4 indicates the wave set-up, short and infragravity significant wave heights at T1-1 for each storm concomitant with spring tide event. The figure 6 shows the wave set-up estimates and the infragravity significant wave height versus the offshore significant wave height associated with the corresponding water levels. The wave set-up and the infragravity
325 significant wave height increase with the offshore significant wave height as expected. The wave setup appears closely related to the water level, with higher wave setup at rising and falling tide whereas at high tide (sea levels > 12 m), the wave set-up is of the order of 10 cm for offshore waves of 4 m. On the contrary, no major correlation is found between the water level and the infragravity significant wave height.

4.2 Implementation of numerical configuration for a local warning coastal flooding system

330 One of the objectives of the PAPI for the Saint Malo Agglomeration is to evaluate the feasibility and interest of setting up a local marine flood forecasting system with respect to the national system. In addition of improving the knowledge of the processes responsible for the flooding in this area, the data presented in this paper are used to build, validate and calibrate hydrodynamic models that could be the basis of this forecasting service. The tide, surge and wave modeling of the French national system are based on the barotropic circulation model Hycom (Baraille and Filatoff, 1995) and on the wave model
335 Wavewatch III (R) (hereinafter WW3, The WAVEWATCH III (R) Development Group, 2016), coupled with the Oasis coupler (Valcke et al., 2015).

The French Atlantic configuration (hereinafter called HR) that is operationally run in the Meteo-France storm surge forecast system has a resolution of 600m at nearshore scale that is insufficient for forecasting flooding at the scale of a city like Saint-Malo. In the context of the PAPI, nested grids for both wave and surge models were generated with resolutions of up
340 to 30 m at the coastline (the same methodology for Pertuis-Charentes is described in (Michaud et al., 2015; Pasquet et al., 2021)). The Oasis coupler was used to provide boundary conditions between the Hycom nested configurations, as well as the coupling between the 30m resolution WW3 and Hycom configurations. The overall system relies on curvilinear grids for Hycom and unstructured grids for WW3. The dedicated topo-bathymetric models presented in this paper were used. The coupling follows the vortex-force approach (Ardhuin et al., 2008; Bennis et al., 2011; Michaud et al., 2012), and the exchanges of all
345 the variables (the current, water level and mask variables from Hycom and sea-state variables from WW3) are done every 10 minutes. This modeling system, called THR, allows to represent some nearshore processes such as wave breaking and wave set-up, thanks to the high resolution and the coupling between models.

Models were calibrated and validated using the series of measurements in Saint-Malo bay (Seyfried et al., 2021). This mod-
350 elling system allow the observation of the wave field transformation at the entrance to Saint-Malo Bay with an eastern part of

the bay highly exposed, and a western part less exposed as it is protected by Cezembre Island (Figure 7.A. for the December 9, 2018 storm at high tide). The significant wave height decreases from the entrance to the bay to the foot of the dykes mainly due to wave breaking in the Saint-Malo bay and interactions with the numerous obstacles (islands, shoals, groynes). The spatial variability of H_{m0} is well represented for this event, as shown by the comparison with observation points. The simulated surge

355 (atmospherical and wave setup) during the December 9 storm at high tide shows a gradient from the open sea to the coast particularly marked close to the shore defences, after the breaking zone (Figure 7.B.), linked to the generation of a wave setup. In the estuary and outer harbor, the effect of the wave setup is negligible. Comparison with the observation points shows an underestimation of the surge offshore, but a good representation of the surge increase at the foot of the structures (moorings T1-1 and T4-1). The model depicts lower surges at certain points in the bay, particularly in some shoals, which are areas of

360 shallow water that induce a shoaling and a set-down. This is also observed at moorings T3-3 and T3-4 which are positioned on shoals, where there are lower surges than at other moorings. However, the resolution of 30 m and uncertainties in data that are of the order of 5 to 10 centimeters, make point-to-point model interpretation and validation difficult.

While being an important process at low tide, simulations and observations reveal that wave setup is negligible at high

365 tide and thus is not a dominant process responsible for coastal flooding (Seyfried et al., 2021). Certain processes, such as infra-gravitational waves or wave over-topping processes that have shown a non-negligible impact on flooding thanks to measurements or observations made during the sea campaign, remain unrepresented in the model. The modelling system developed in this study is thus non sufficient and would need to be complemented at nearshore scale by a phase-resolved model to represent the infra-gravity waves as well as over-topping. Additional measurements would thus be necessary to calibrate and validate

370 this phase-resolved model and in particular with cameras, pressure gauges or lidar stations on the dyke.
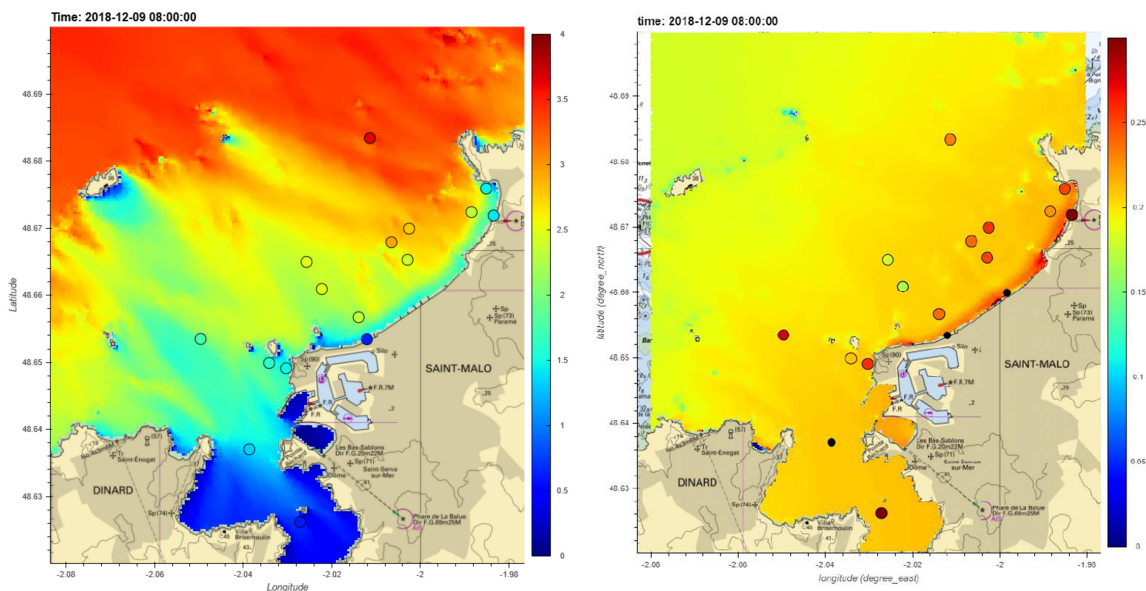
Figure 7. Map of significant wave height (up) and surge (atmospherical and wave setup) (bottom) in meters at high tide simulated by the THR system during the December 9, 2018 storm. The color of dots represents the measured value at the various moorings during this event.

5   Data availability

The TBDTMs (SHOM, 2020a, b) and oceanographic datasets (SHOM, 2021) are freely available at doi :

– https://doi.org/10.17183/MNT_COTIER_GNB_PAPI_SM_20m_WGS84

– https://doi.org/10.17183/MNT_COTIER_PORT_SM_PAPI_SM_5m_WGS84

375   – https://doi.org/10.17183/CAMPAGNE_OCEANO_STMALO

TBDTMs is released through pre-packed files, including:

– files containing bathymetric surfaces, vertically referenced to different vertical datums (Mean Sea Level or Lowest Astronomical Tide) and converted in four grid formats, including NetCDF format (.grd by GMT), Bathymetric Attributed Grid (.bag), ESRI ASCII Raster format (.asc) and ascii text format (.glz)

380   – a metadata file that contains data sources, geographical extent, legal constraints and a brief summary of the building process, meeting the requirements of the INSPIRE Directive;

- the citation and an associated Digital Object Identifier (unique identifier used to cite scientific articles and datasets) to easily identify the future multiple uses of the DTM;

- the rights and contents report describing the main features of the product and its limitation of use.

385 Oceanographic dataset is available through four levels of processing, including :

- L0 : direct output of sensors at binary or ascii format.

- L1 : processed outputs of sensors at ascii format using the manufacturers' software.

- L2 : processed data and metadata at NetCDF format.

- L3 : post-processed integrated or peak to peak wave parameters at NetCDF format.

390 6 Conclusions

The acquisition of new topo-bathymetric data in the Bay of Saint-Malo allowed the creation of a topo-bathymetric dataset. This dataset contains two TBDTMs with a resolution of 20 m and 5 m, respectively. An extensive oceanographic campaign was also carried out to create a dataset that provides a set of oceanographic parameters (water levels, currents and sea states) in the Bay of Saint-Malo for different atmospheric, tidal and sea states conditions.

395

During the oceanographic campaign, three moderate storms occurred in the Bay of Saint-Malo. The dataset allows the evaluation of the different oceanographic processes involved in coastal flooding. This dataset provides, for the first time, a measurement of the wave transformation in the bay of Saint-Malo. It also provides a quantification of the wave processes at the foot of the protection structures. In this macro-tidal area, the variation of the water level plays a major role on wave pro-

400 cesses. At high spring tide, the short and the infragravity waves spread up to the protection structures. The wave set-up is not established, but overtopping by sea pack can occur (not measured).

Topo-bathymetric and oceanographic datasets are useful to build, validate and calibrate wave and hydrodynamic models. In the context of the PAPI, a local coastal flood system has been developped to reproduce the surge and waves at high resolution

405 in the Saint-Malo bay. Comparison and calibration with measurements have been made and show that this high-resolution model therefore clearly improves the representation of wave dissipation and surge in the bay, and therefore the national marine flood forecasting system. It provides the right information, refined in resolution and precision, to set up a first level of impact indicators on a local scale. However, some observed processes, such as infra-gravitational waves, wave over-topping remain unrepresented in the model. The coupled system is thus the essential link in the chain to complete the coastal forecasting ca-

410 pability with a phase-resolved model that would enable the modelling of all the processes responsible for a potential flooding event.

Finally, although this type of dataset are costly to build and limited in space and time, it allows to characterize processes at short scales and therefore appears complementary to the increasing monitoring of coastal variables by means of satellite
415 altimeters which face strong limitations in coastal area.

Appendix A: Surface elevation reconstruction method from bottom pressure

Three different reconstruction methods were used.

A1 Hydrostatic reconstruction

The hydrostatic reconstruction based on the hydrostatic equilibrium (Eq. A1).

420 $$\zeta_h = h - h_0 + \delta_m \tag{A1}$$

with ζ_h, the hydrostatic free surface elevation (in m), h_0 the mean water depth (in m) and δ_m the sensor's distance from bed (in m).

A2 Linear reconstruction

The linear reconstruction based on a transfer function derived from the linear wave theory (TFM) is the most commonly used
425 method (e.g., see Bishop and Donelan, 1987).

$$F\{\zeta_{linear}\} = K_p(\omega)F\{\zeta_h\} \tag{A2}$$

where $F\{\cdot\}$ corresponds to the Fourier transform and $K_p(\omega)$ is the transfer function:

$$K_p(\omega) = \frac{\cosh(k(\omega)h_0)}{\cosh(k(\omega)\delta_m)} \tag{A3}$$

Solving this equation requires the use of the dispersion relation issued from the linear wave theory:

430 $$\omega^2 = gk\tanh(kh_0) \tag{A4}$$

This method requires an upper cutoff frequency so as to remove high frequency noise that is amplified by the transfer function and to prevent the over-amplification of high frequency energy levels due to non-linear interactions in intermediate and shallow waters (e.g. see Bonneton and Lannes, 2017; Bonneton et al., 2018; Mouragues et al., 2019; Martins et al., 2020). For frequencies exceeding the limit frequency, the correction factor can be replaced by different values: $K_p = 1$ (sharp cut-off, the
435 linear spectrum is replaced by hydrostatic spectrum), linear correction factor, steady correction factor and Jonswap spectrum (see Mouragues et al., 2019, for description of these methods). The optimization of the cut-off frequency and correction factor are a source of improvement in the representation of the wave shape (Mouragues et al., 2019; Martins et al., 2020). In this study, in order to simplify the treatment and make it homogeneous, a sharp cut-off frequency of 0.25 Hz was chosen for the whole dataset.

A3   Non-linear weakly dispersive reconstruction

The nonlinear weakly dispersive (swnl) reconstruction (Eq. A5) was introduced by Bonneton et al. (2018). This method consists of reconstructing surface wave elevation from non-linear wave theory for weakly dispersive waves.

$$\zeta_{swnl} = \zeta_{swl} - \frac{1}{g}\left[\partial_t(\zeta_{swl}\partial_t\zeta_{swl}) - (\frac{\delta_m}{h_0})^2(\partial_t\zeta_{swl})^2\right] \tag{A5}$$

with ζ_{swl}, the free surface elevation from the linear weakly dispersive reconstruction :

$$\zeta_{swl} = \zeta_h - \frac{h_0}{2g}\left[1 - (\frac{\delta_m}{h_0})^2\right]\partial_t^2\zeta_h \tag{A6}$$

As opposed to the TFM, the resolution of Eq.A5 does not require the use of a dispersion relationship. However, this transform requires intrusion of cutoff frequency to filter the measurement noise (Mouragues et al., 2019). In this study, in order to simplify the treatment and make it homogeneous, a cut-off frequency of $0.5 Hz$ was chosen for the whole dataset. This method allows a better reconstruction of the height of the highest waves near the breaking point (Mouragues et al., 2019), however its application is limited to a weakly dispersive wave regime.

A comparison of free surface elevation with the different methods and with the AST acquisition is shown in figure A1 for high and low tide. H_{m0} is also given for the different methods and sensors.

Appendix B: Bulk parameters: spectral estimates and wave-by-wave analysis

The spectral significant wave height(H_{m0}), mean periods (T_{m0n}) and continuous peak period (T_{pc}) were computed using using the $n-th$ moment of the wave spectra (E corresponding to the power spectral density of the elevation signal), which reads:

$$m_n = \int\limits_{f_{min}}^{f_{max}} f^n E(f)df \tag{B1}$$

such that:

$$H_{m0} = 4\sqrt{m_0} \tag{B2}$$

$$T_{m_{0n}} = \left(\frac{m_0}{m_n}\right)^{1/n} \tag{B3}$$

$$T_{pc} = \frac{m_{-2}m_1}{m_0^2} \tag{B4}$$

while the discrete peak period was computed from the spectral maximum at the peak frequency f_{peak}, as $T_{peak} = 1/f_{peak}$. As an initial approach, the lower bound f_{min} used for computing the moments of the wave spectra was set to 0.04 Hz, note
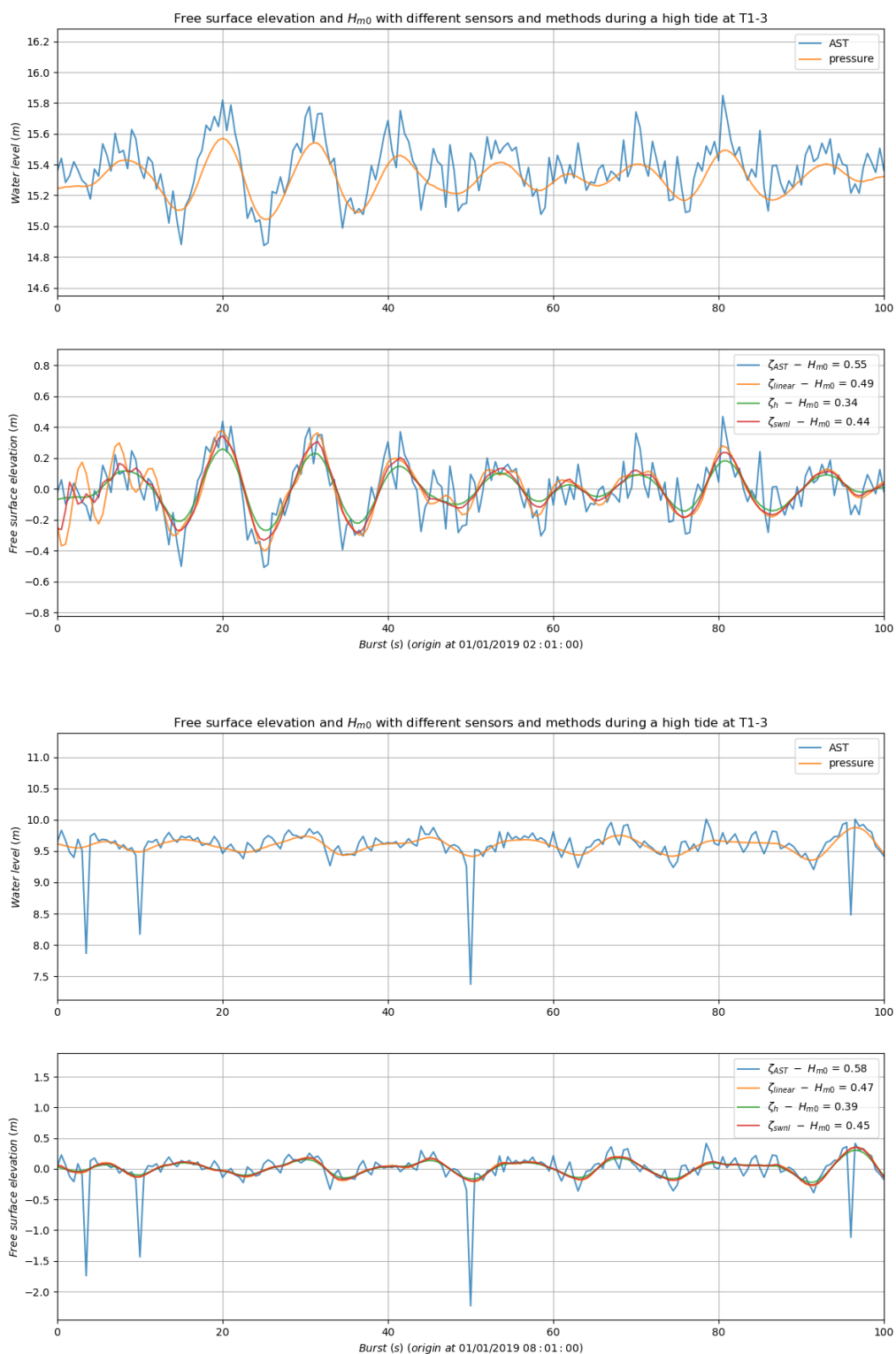
Figure A1. Comparison of free surface elevation with the different methods and with the AST acquisition for high (up) and low (bottom) tide. The value of H_{m0} is also given for the different methods

however that a convenient separation between the infragravity band and the gravity band might be defined as half the offshore peak frequency (e.g. see Hamm and Peronnard, 1997; Bertin et al., 2020). The upper bound f_{max} was consistently set to $f_c = 0.2\,\text{Hz}$ for wave pressure gauge and $0.4\,\text{Hz}$ for the wave buoys and the AWAC.

470   Considering a well-sampled and detrended timeseries of free surface elevation, an individual wave is defined by convention as the elevation profile between two consecutive instants of downward zero crossing. The height (H) of an individual wave is then defined as the difference between the maximum (the crest) and minimum (the trough) values of elevation, while the period (T) is the time separating the final instant from the initial instant. In practice a peak is defined as any sample whose two direct neighbours have a smaller amplitude with a minimum distance between two peaks roughly corresponding to a minimum

475   period set to 4 s and a minimum amplitude ($\simeq H/2$) set to 0.1 m. For flat peaks (i.e. more than one sample of equal amplitude wide) the index of the middle sample is returned, rounded down in case the number of samples is even. Given the minimum period and the length of a burst, one can estimate the upper limit of observable waves per burst. If the number of waves actually detected does not exceed 10%, the burst is rejected. For N waves detected in the timeseries, the mean wave height ($\overline{H}$) and mean wave period ($\overline{T}$) are given by:

$$\overline{H} = \frac{1}{N} \sum_{i=1}^{N} H_i \tag{B5}$$

$$\overline{T} = \frac{1}{N} \sum_{i=1}^{N} T_i \tag{B6}$$

The significant wave height is computed as the mean value of the top one-third largest waves in the distribution:

$$H_{1/3} = \frac{1}{N/3} \sum_{j=2N/3}^{N} H_j \tag{B7}$$

485   where j is the index of the waves sorted in ascending order. The maximal wave height (H_{max}) is also computed from the wave-by-wave analysis:

$$H_{max} = \max_{i \in [\![1,N]\!]} (H_i) \tag{B8}$$

Appendix C: Calibration and relocation of the pressure sensors

Calibration is done differently for offshore and foreshore sensors. One solution would be to calibrate them in a laboratory

490   beforehand but pressure sensors are really sensitive to temperature shocks. Transports to the field site can take several weeks or months if it is made by boat, rendering the prior calibration unusable. Another solution is to compare and adjust the data with the atmospheric pressure measurements and this is done easily with sensors on the foreshore, that are pulled out of the water twice a day. For offshore sensors, the only way is to looked at the data before or after being moored.

Another difficulty is in the vertical relocation of the instruments. The vertical positions of the foreshore instruments is
495 obtained with DGPS, whereas the offshore ones are obtained with the sonar ship. To compare the different measurements, one
solution is to relocate them in height with respect to the tide gauge of Saint-Malo harbour. Correction factors (slope and offset)
from Saint-Malo tide gauge is calculated for each sensor.

Author contributions. HM, LB, AP and FL designed the field experiments. LB produced the TBDTMs. LS, HM and MP produced the
oceanographic dataset. LS, HM and LB prepared the paper, with contributions from all co-authors.

500 *Competing interests.* The authors declare that they have no conflict of interest.

Acknowledgements. The authors would like to thank the Shom GHOA, IES and Altimétrie littorale teams and all those who participated in
the measurement campaign. This research is supported by Shom, Saint-Malo, SMA, Departmental Council of Ille et Vilaine (CD35), Brittany
region and the French State. This research is also supported by PROTEVS research program funded by DGA and conducted by Shom. The
Litto3D coastal elevation model used for this study is co-produced by IGN and Shom.

References

Amante, C. J.: Accuracy of interpolated bathymetric digital elevation models, Ph.D. thesis, University of Colorado at Boulder, 2012.

Ardhuin, F., Rascle, N., and Belibassakis, K.: Explicit wave-averaged primitive equations using a generalized Lagrangian mean., Ocean Modelling, 20, 35–60, 2008.

Baraille, R. and Filatoff, N.: Modèle shallow-water multicouches isopycnal de Miami, Tech. Rep. 003/95, Shom, 1995.

Bennis, A., Ardhuin, F., and Dumas, F.: On the coupling of wave and three-dimensional circulation models : Choice of theoretical framework, pratical implementation and adiabatic tests, Ocean Modelling, 40, 260–272, 2011.

Bertin, X., Bruneau, N., Breilh, J.-F., Fortunato, A. B., and Karpytchev, M.: Importance of wave age and resonance in storm surges: The case Xynthia, Bay of Biscay, Ocean Modelling, 42, 16–30, 2012.

Bertin, X., Martins, K., de Bakker, A., Chataigner, T., Guérin, T., Coulombier, T., and de Viron, O.: Energy transfers and reflection of infragravity waves at a dissipative beach under storm waves, Journal of Geophysical Research: Oceans, 125, e2019JC015 714, 2020.

Biscara, L., Maspataud, A., and Schmitt, T.: Generation of bathymetric digital elevation models along French coasts: Coastal risk assessment, Hydro Int, 20, 26–29, 2016.

Bishop, C. T. and Donelan, M. A.: Measuring waves with pressure transducers, Coastal Engineering, 11, 309–328, https://doi.org/10.1016/0378-3839(87)90031-7, 1987.

Bonneton, P. and Lannes, D.: Recovering water wave elevation from pressure measurements, Journal of Fluid Mechanics, 833, 399–429, https://doi.org/10.1017/jfm.2017.666, 2017.

Bonneton, P., Lannes, D., Martins, K., and Michallet, H.: A nonlinear weakly dispersive method for recovering the elevation of irrotational surface waves from pressure measurements, Coastal Engineering, 138, 1–8, https://doi.org/10.1016/j.coastaleng.2018.04.005, 2018.

Bonnot-Courtois, C.: Bay of Mont-Saint-Michel and the Rance Estuary: Recent Development and Evolution of the Depositional Environments, vol. 26, Editions Technip, 2002.

Cariolet, J.: Inondation des côtes basses et risque associés en Bretagne: vers un redéfinition des processus hydrodynamiques liés aux conditions météo-océaniques et des paramètres morpho-sédimentaires, Ph.D. thesis, Brest University, 2011.

Caspar, R., Costa, S., and Jacob, E.: Fronts froids et submersions de tempêtes dans le nord-ouest de la France : le cas des inondations par la mer entre l'estuaire de la Seine et de la Somme, La Météorologie, 57, 37–47, 2007.

Cochet, C. and Lambert, M.: The Rance tidal power plant model, in: In Proceedings of the XXIVth TELEMAC-MASCARET User Conference, 17 to 20 October 2017, Graz University of Technology, Austria, pp. 191–196, 2017.

Conrad, O., Bechtel, B., Bock, M., Dietrich, H., Fischer, E., Gerlitz, L., Wehberg, J., Wichmann, V., and Böhner, J.: System for Automated Geoscientific Analyses (SAGA) v. 2.1.4, Geoscientific Model Development, 8, 1991–2007, https://doi.org/10.5194/gmd-8-1991-2015, 2015.

Crossland, C. J., Kremer, H. H., Lindeboom, H. J., Crossland, J. I. M., and Tissier, M. D. A. L., eds.: Coastal Fluxes in the Anthropocene, Springer Berlin Heidelberg, https://doi.org/10.1007/3-540-27851-6, 2005.

Dagorne, A.: Contribution à l'étude géomorphologique et sédimentologique du littoral de la région de Dinard-Saint-Briac (Ille-et-Vilaine), Ph.D. thesis, Rennes University, 1966.

Dagorne, A.: Le sud du golfe normand-breton: carte sédimentologique des fonds détritiques du prélittoral et répartition du calcaire organogène total., Tech. rep., Doc. Lab. Géomorphologie Dinard, 2., 1968.

Danielson, J. J., Poppenga, S. K., Brock, J. C., Evans, G. A., Tyler, D. J., Gesch, D. B., Thatcher, C. A., and Barras, J. A.: Topobathymetric Elevation Model Development using a New Methodology: Coastal National Elevation Database, Journal of Coastal Research, 76, 75–89, https://doi.org/10.2112/si76-008, 2016.

DHI: Plan de prévention des risques littoraux de Saint Malo, Rapport de phase 2, Tech. rep., DHI, 2016.

545 Dodet, G., Leckler, F., Sous, D., Ardhuin, F., Filipot, J., and Suanez, S.: Wave Runup Over Steep Rocky Cliffs, Journal of Geophysical Research: Oceans, 123, 7185–7205, https://doi.org/10.1029/2018jc013967, 2018.

Dodet, G., Melet, A., Ardhuin, F., Bertin, X., Idier, D., and Almar, R.: The Contribution of Wind-Generated Waves to Coastal Sea-Level Changes, Surveys in Geophysics, 40, 1563–1601, https://doi.org/10.1007/s10712-019-09557-5, 2019.

Eakins, B. and Taylor, L.: Seamlessly integrating bathymetric and topographic data to support tsunami modeling and forecasting efforts, 550 Ocean globe, pp. 37–56, 2010.

Eakins, B. W. and Grothe, P. R.: Challenges in Building Coastal Digital Elevation Models, Journal of Coastal Research, 297, 942–953, https://doi.org/10.2112/jcoastres-d-13-00192.1, 2014.

Eakins, B. W., Taylor, L. A., Carignan, K. S., and Kenny, M. R.: Advances in Coastal Digital Elevation Models, Eos, Transactions American Geophysical Union, 92, 149–150, https://doi.org/10.1029/2011eo180001, 2011.

555 Famin, V., Michon, L., and Bourhane, A.: The Comoros archipelago: a right-lateral transform boundary between the Somalia and Lwandle plates, Tectonophysics, 789, 228 539, https://doi.org/10.1016/j.tecto.2020.228539, 2020.

Filipot, J.-F., Roeber, V., Boutet, M., Ody, C., Lathuiliere, C., Louazel, S., Schmitt, T., Ardhuin, F., Lusven, A., Outré, M., et al.: Nearshore wave processes in the Iroise Sea: field measurements and modelling, in: Coastal Dynamics 2013-7th International Conference on Coastal Dynamics, http://www. coastaldynamics2013. fr/pdf_files/055_Filipot_Jean_Francois. pdf, pp. p–605, 2013.

560 Fox-Kemper, B., Hewitt, H., Xiao, C., Aðalgeirsdóttir, G., Drijfhout, S., Edwards, T., Golledge, N., Hemer, M., Kopp, R., Krinner, G., Mix, A., Notz, D., Nowicki, S., Nurhati, I., Ruiz, L., Sallée, J.-B., Slangen, A., and Yu, Y.: 2021: Ocean, Cryosphere and Sea Level Change. In Climate Change 2021: The Physical Science Basis. Contribution of Working Group I to the Sixth Assessment Report of the Intergovernmental Panel on Climate Change, Cambridge University Press, Cambridge, United Kingdom and New York, NY, USA, https://doi.org/10.1017/9781009157896.011, 2021.

565 Furgerot, L., Poprawski, Y., Violet, M., Poizot, E., du Bois, P. B., Morillon, M., and Mear, Y.: High-resolution bathymetry of the Alderney Race and its geological and sedimentological description (Raz Blanchard, northwest France), Journal of Maps, 15, 708–718, https://doi.org/10.1080/17445647.2019.1657510, 2019.

Gesch, D. and Wilson, R.: Development of a Seamless Multisource Topographic/Bathymetric Elevation Model of Tampa Bay, Marine Technology Society Journal, 35, 58–64, https://doi.org/10.4031/002533201788058062, 2001.

570 Hamm, L. and Peronnard, C.: Wave parameters in the nearshore: A clarification, Coastal Engineering, 32, 119 – 135, 1997.

Hébert, H., Abadie, S., Benoit, M., Créach, R., Frère, A., Gailler, A., Garzaglia, S., Hayashi, Y., Loevenbruck, A., Macary, O., et al.: Project TANDEM (Tsunamis in the Atlantic and the English ChaNnel: Definition of the Effects through numerical Modeling)(2014-2018): a French initiative to draw lessons from the Tohoku-oki tsunami on French coastal nuclear facilities, in: EGU General Assembly Conference Abstracts, p. 6421, 2014.

575 IHO: IHO Standards for Hydrographic Surveys (Edition 5, 2008), Tech. rep., IHO, https://iho.int/uploads/user/pubs/standards/s-44/S-44_5E. pdf, 2017a.

IHO: Standards of Competence for Category "B" Hydrographic Surveyors (Edition 1.0.1, June 2017), Tech. rep., IHO, https://iho.int/uploads/user/pubs/standards/s-5/S-5B_Ed1.0.1.pdf, 2017b.

IHO: Standards of Competence for Category "A" Hydrographic Surveyors (Edition 1.0.2, June 2018), Tech. rep., IHO, https://iho.int/uploads/
580   user/pubs/standards/s-5/S-5A_Ed1.0.2.pdf, 2018.

Jourdan, D., Paradis, D., Pasquet, A., Michaud, H., Baraille, R., Biscara, L., Dalphinet, A., and Ohl, P.: La phase-3 du projet HOMONIM :
       définition et contenu, in: XVIèmes Journées, Le Havre, Editions Paralia, https://doi.org/10.5150/jngcgc.2020.087, 2020.

Krogstad, H. E., Gordon, R. L., and Miller, M. C.: High-resolution directional wave spectra from horizontally mounted acoustic Doppler
       current meters, Journal of Atmospheric and Oceanic Technology, 5, 340–352, 1988.

585   Le Deunf, J., Schmitt, T., Keramoal, Y., Jarno, R., and Fally, M.: Automating the Management of 300 Years of Ocean Mapping Effort in
       Order to Improve the Production of Nautical Cartography and Bathymetric Products: Shom's Téthys Workflow., Geomatics, 3, 239–249,
       https://doi.org/10.3390/jmse8110847, 2023.

Le Menn, M. and Morvan, S.: Velocity Calibration of Doppler Current Profiler Transducers, Journal of Marine Science and Engineering, 8,
       847, https://doi.org/10.3390/jmse8110847, 2020.

590   Louvart, L. and Grateau, C.: The Litto3D project, in: Europe Oceans 2005, IEEE, https://doi.org/10.1109/oceanse.2005.1513237, 2005.

Macnab, R. and Jakobsson, M.: Something old, something new: compiling historic and contemporary data to construct regional bathymetric
       maps, with the Arctic Ocean as a case study, The International Hydrographic Review, 2000.

Martins, K., Bonneton, P., Mouragues, A., and Castelle, B.: Non-hydrostatic, Non-linear Processes in the Surf Zone, Journal of Geophysical
       Research: Oceans, 125, https://doi.org/10.1029/2019jc015521, 2020.

595   Maspataud, A., Biscara, L., Hébert, H., Schmitt, T., and Créach, R.: Coastal Digital Elevation Models (DEMs) for tsunami hazard assessment
       on the French coasts, in: EGU General Assembly Conference Abstracts, p. 1590, 2015.

Melet, A., Teatini, P., Cozannet, G. L., Jamet, C., Conversi, A., Benveniste, J., and Almar, R.: Earth Observations for Monitoring Marine
       Coastal Hazards and Their Drivers, Surveys in Geophysics, 41, 1489–1534, https://doi.org/10.1007/s10712-020-09594-5, 2020.

Michaud, H., Marsaleix, P., Leredde, Y., Estournel, C., Bourrin, F., Lyard, F., Mayet, C., and Ardhuin, F.: Three-dimensional modelling of
600   wave-induced current from the surf zone to the inner shelf, Ocean Science, 8, 657–681, https://doi.org/10.5194/os-8-657-2012, 2012.

Michaud, H., Pasquet, A., Baraille, R., Leckler, F., Aouf, A., Dalphinet, A., Huchet, M., Roland, A., Dutour-Sikiric, M., Ardhuin, F., and
       Filipot, J.: Implementation of the new French operational coastal wave forecasting system and application to a wave-current interaction
       study, in: 14th International Workshop on Wave Hindcasting and Forecasting & 5th Coastal Hazard Symposium, 2015.

Mouragues, A., Bonneton, P., Lannes, D., Castelle, B., and Marieu, V.: Field data-based evaluation of methods for recovering surface wave
605   elevation from pressure measurements, Coastal Engineering, 150, 147–159, https://doi.org/10.1016/j.coastaleng.2019.04.006, 2019.

Oltman-Shay, J. and Guza, R.: A data-adaptive ocean wave directional-spectrum estimator for pitch and roll type measurements, Journal of
       physical oceanography, 14, 1800–1810, 1984.

Pasquet, A., Michaud, H., Seyfried, L., Baraille, R., Biscara, L., Y., K., and Jourdan, D.: Improving storm surge and wave forecasts from
       regional to nearshore scales, in: 9th EuroGOOS Conference, 2021.

610   Pastol, Y.: Use of Airborne LIDAR Bathymetry for Coastal Hydrographic Surveying: The French Experience, Journal of Coastal Research,
       62, 6–18, https://doi.org/10.2112/si_62_2, 2011.

Seyfried, L., Michaud, H., and Pasquet, A.: Réanalyse et modélisation des surcotes et états de mer, Livrable Shom n°4, PAPI Saint-Malo,
       Axe 2, Action 2.I, Tech. rep., Shom, 2021.

SHOM: MNT   topo-bathymétrique   côtier   d'une   partie   du   golfe   normand-breton   (PAPI   Saint-Malo),
615   https://doi.org/10.17183/MNT_COTIER_GNB_PAPI_SM_20M_WGS84, 2020a.

SHOM: MNT topo-bathymétrique côtier du port de Saint-Malo et de ses abords (PAPI Saint-Malo), https://doi.org/10.17183/MNT_COTIER_PORT_SM_PAPI_SM_5M_WGS84, 2020b.

SHOM: Sea cruise French Flooding Prevention Action Program of Saint-Malo, https://doi.org/10.17183/CAMPAGNE_OCEANO_STMALO, 2021.

620 Tawil, T. E., Guillou, N., Charpentier, J.-F., and Benbouzid, M.: On Tidal Current Velocity Vector Time Series Prediction: A Comparative Study for a French High Tidal Energy Potential Site, Journal of Marine Science and Engineering, 7, 46, https://doi.org/10.3390/jmse7020046, 2019.

Tew-Kai, E., Quilfen, V., Cachera, M., and Boutet, M.: Dynamic Coastal-Shelf Seascapes to Support Marine Policies Using Operational Coastal Oceanography: The French Example, Journal of Marine Science and Engineering, 8, 585, https://doi.org/10.3390/jmse8080585, 625 2020.

The WAVEWATCH III (R) Development Group: User manual and system documentation of WAVEWATCH III R version 5.16. Tech. Note 329, NOAA/NWS/NCEP/MMAB, College Park, MD, USA, 326 pp. + Appendices., 2016.

Valcke, S., Craig, T., and Coquart, L.: OASIS3-MCT User Guide, OASIS3-MCT 3.0, Tech. Rep. TR/CMGC/15/38, CERFACS/CNRS SUC URA No1875, Toulouse, France, 2015.

630 Wong, A. M., Campagnoli, J. G., and Cole, M. A.: Assessing 155 Years of Hydrographic Survey Data for High Resolution Bathymetry Grids, in: OCEANS 2007, IEEE, https://doi.org/10.1109/oceans.2007.4449373, 2007.

Woodworth, P. L., Melet, A., Marcos, M., Ray, R. D., Wöppelmann, G., Sasaki, Y. N., Cirano, M., Hibbert, A., Huthnance, J. M., Monserrat, S., and Merrifield, M. A.: Forcing Factors Affecting Sea Level Changes at the Coast, Surveys in Geophysics, 40, 1351–1397, https://doi.org/10.1007/s10712-019-09531-1, 2019.